



The Menace of Momentum: Dynamic Forces on Flexible Organisms

Mark Denny; Brian Gaylord; Brian Helmuth; Tom Daniel

Limnology and Oceanography, Vol. 43, No. 5 (Jul., 1998), 955-968.

Stable URL:

<http://links.jstor.org/sici?sici=0024-3590%28199807%2943%3A5%3C955%3ATMOMDF%3E2.0.CO%3B2-7>

Limnology and Oceanography is currently published by American Society of Limnology and Oceanography.

Your use of the JSTOR archive indicates your acceptance of JSTOR's Terms and Conditions of Use, available at <http://www.jstor.org/about/terms.html>. JSTOR's Terms and Conditions of Use provides, in part, that unless you have obtained prior permission, you may not download an entire issue of a journal or multiple copies of articles, and you may use content in the JSTOR archive only for your personal, non-commercial use.

Please contact the publisher regarding any further use of this work. Publisher contact information may be obtained at <http://www.jstor.org/journals/limnoc.html>.

Each copy of any part of a JSTOR transmission must contain the same copyright notice that appears on the screen or printed page of such transmission.

JSTOR is an independent not-for-profit organization dedicated to creating and preserving a digital archive of scholarly journals. For more information regarding JSTOR, please contact jstor-info@umich.edu.

The menace of momentum: Dynamic forces on flexible organisms

Mark Denny and Brian Gaylord

Department of Biological Sciences, Stanford University, Hopkins Marine Station, Pacific Grove, California 93950

Brian Helmuth and Tom Daniel

University of Washington, Department of Zoology, Box 351800, Seattle, Washington 98195-1800

Abstract

It has been proposed that the mechanical flexibility of many wave-swept organisms reduces the hydrodynamic forces imposed on these plants and animals. For example, reorientation of the organism can render it more streamlined, and by “going with the flow” a flexible organism can reduce the relative velocity between itself and the surrounding water, thereby reducing drag and lift. Motion of the body allows the organism to gain momentum, however, and this momentum can apply an inertial force when the organism’s motion is slowed by the deformation of the body’s supporting structures. Through a series of mathematical models we show that the inertial forces imposed on flexible plants and animals can be large enough to increase the overall force on the organism, more than offsetting the advantages of moving with the flow. A dimensionless index, the *jerk number*, is proposed as a tool for predicting when inertial forces will be important, and the utility of this index is explored through an examination of the forces applied to kelps and mussels. The tendency for inertial loading to peak at certain frequencies raises the possibility that the structure of organisms can be tuned (either by evolution or physiological response) to avoid potentially damaging loads.

Benthic marine organisms in the intertidal and shallow subtidal zones must contend with harsh and oftentimes highly variable environmental conditions. At sites exposed to wave action, wave-induced hydrodynamic forces can be the dominant environmental stress. For example, water velocities in breaking waves commonly reach values of 10 ms^{-1} , resulting in the imposition of large forces on benthic organisms (e.g. Denny et al. 1985; Denny 1988; Gaylord et al. 1994; Denny 1995). Whenever the supporting structure of a creature is insufficient to resist these forces, mechanical failure occurs and the organism is tattered, broken, or dislodged from the substratum.

Previous studies have shown that differential susceptibility to physical disturbance can have profound influences on an individual’s survival, the distribution of species across habitats, and the structure of the biotic community as a whole (e.g. Dayton 1971; Paine and Levin 1981; Sousa 1979a,b; Menge 1978). A mechanistic, quantitative examination of the forces imposed on organisms in the marine environment and the means by which these organisms contend with these forces is therefore crucial to understanding the morphology, physiology, ecology, and evolution of organisms on wave-swept shores.

The interaction between the supporting structures of benthic organisms and the hydrodynamic forces of the environment, however, is poorly understood. Specifically, most previous studies examining the forces imposed on organisms in high-energy environments have assumed that the organism is stationary (e.g. Koehl 1977a; Denny et al. 1985; Carrington 1990; Denny 1993, 1994; Gaylord et al. 1994). Although this is reasonable for rigid organisms rigidly adherent to the substratum, it may not be appropriate for flexible plants and animals (such as anemones, hydrozoans, mussels, gooseneck barnacles, soft corals, and most macroalgae) that are able to reorient and move with the flow.

This ability has three pertinent consequences. First, the deformation and reorientation of the organism may render it more streamlined. Second, the motion of the organism as it deforms can change (and often reduce) the velocity and acceleration of the fluid relative to the plant or animal. By assuming a less resistive posture and moving with the flow, the organism may reduce the hydrodynamic forces imposed upon it. Third, motion of the body allows the organism to gain momentum. This momentum can, in turn, apply an inertial force to the body when the body’s motion is slowed by any elastic attachment to the stationary substratum. Thus, movement, as determined by the properties of a plant or animal’s supporting structure, can potentially affect the total force applied to the organism. Although a few studies have investigated the effects of the mechanical properties of supports on the forces they experience (e.g. Koehl 1977a,b), as well as the significance of bending in flow on drag coefficients and projected surface area (see Gaylord et al. [1994] and the references cited therein), the potential importance of flexibility has not yet been thoroughly explored.

An important issue here relates to the rather tacit assumption that movement in flow confers lower forces than would be encountered by stationary creatures. To address this issue explicitly, we present a sequence of mathematical models that quantitatively explore the inertial consequences of flexibility. Here, these models are applied to the particular case of benthic organisms in the wave-swept environment where the fluid (seawater) is dense, the velocities and accelerations may be large, and the hydrodynamic forces can therefore be substantial. The same principles apply, however, for plants and animals in a wide variety of other habitats.

Hydrodynamic versus inertial forces

Consider first what is often the largest hydrodynamic force, *drag*, a force acting in the direction of flow (Vogel 1994). For flow along the x -axis:

$$\text{Drag} = \frac{1}{2} \rho C_d A u_{x,r} |u_{x,r}|, \quad (1)$$

where the relative velocity, $u_{x,r}$, is

$$u_{x,r} = u_x - \frac{dx}{dt}. \quad (2)$$

Here, u_x is the velocity of the water and dx/dt is the velocity of the organism (both measured relative to the stationary substratum), ρ is the density of the fluid (for our purposes the density of seawater, nominally $1,025 \text{ kg m}^{-3}$), C_d is the drag coefficient (a function of shape and Reynolds number), and A is the maximal projected area of the object.

A similar expression describes *lift*, a force perpendicular to the direction of flow (Vogel 1994; Denny 1988):

$$\text{Lift} = \frac{1}{2} \rho C_l A u_{x,r} |u_{x,r}|. \quad (3)$$

Here, C_l is the dimensionless lift coefficient.

Because these forces depend on the magnitude of flow relative to the plant or animal, if the organism moves with the flow, the imposed hydrodynamic force is reduced. In this respect, flexibility of the organism is advantageous—it allows the organism to “go with the flow.”

There is a tradeoff involved with this motion, however. If the body (or some portion of it) moves with the fluid, the moving mass acquires momentum. For a body of finite length attached to the substratum, at some point in its travel the mass of the body must be brought to a halt by the resistive deflection of the body. This process, which necessarily entails a change in the body’s momentum, results in the imposition of an *inertial force*, governed by the rate at which the body is decelerated:

$$\text{Inertial force} = \frac{d}{dt} \left(m \frac{dx}{dt} \right), \quad (4)$$

where m is the effective mass of the moving body.

Size and flexibility can therefore have strong effects on the ratio of inertial to hydrodynamic forces. A large, flexible structure can move with the flow for a time, thereby reducing drag and lift. But this reduction in force can be had only at the expense of acquiring momentum, and the bill must be paid by the imposition of an inertial force when the structure can no longer freely follow the flow.

We approach an understanding of the roles of static and dynamic stresses through the use of three simple mathematical models that embody several major principles. These models are in some respects simplistic and are not intended to portray a precise picture of the real world. They are, however, instructive. Once the basic principles have been established using these models, we examine three models of greater complexity that deal with specific biological examples from the wave-swept environment. In the process, several additional aspects of the dynamics of wave-swept organisms are introduced. These more realistic (although still somewhat simplistic) models allow us to explore how well the principles gleaned from the simple heuristic models are likely to apply in nature.

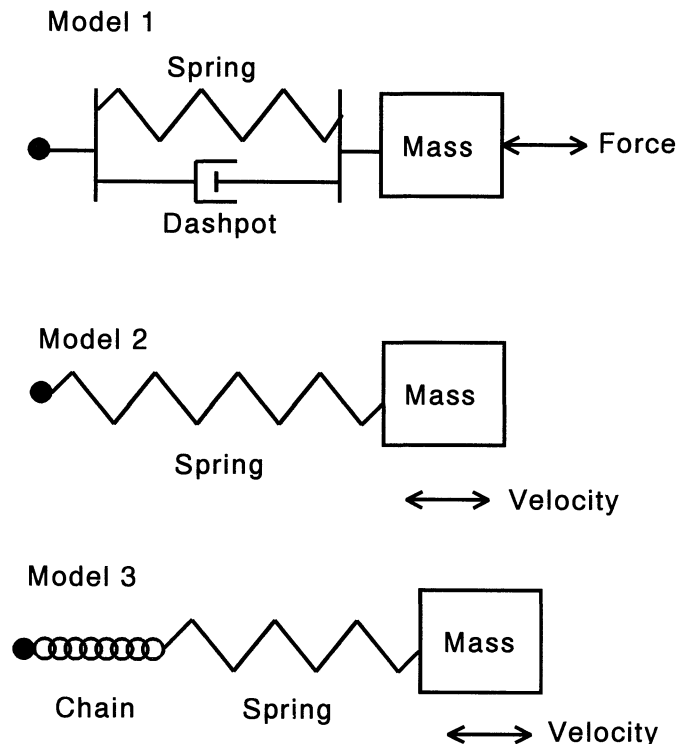


Fig. 1. Schematic diagrams of the three heuristic models. See text for details.

Model 1: A mass on a damped spring

The motion of a mass held in place by a damped spring and subjected to a force that varies sinusoidally through time (Fig. 1A) can be described (in one dimension) by the relationship (Thomson 1993)

$$m \left(\frac{d^2x}{dt^2} \right) + b \left(\frac{dx}{dt} \right) + kx = W \sin \omega t, \quad (5)$$

where m is the mass of the object, x is its location along the axis of motion, t is time, b is the damping coefficient (a measure of the rate at which energy is lost to friction), and k is the stiffness of the spring (force per deflection). W is the amplitude of the external force applied to the system, and ω is the radian frequency of the force’s oscillation ($\omega = 2\pi/T$, where T is the period of the force’s oscillation).

Dimensional analysis of this relationship reveals that four dimensionless variables are required for a complete description of the system’s motion. The first of these is F , the ratio of the actual maximum force imposed on the system by its deflection to the peak external force applied. In this case

$$F = \frac{kx_m}{W}, \quad (6a)$$

where x_m is the maximum deflection. In the absence of dynamic (that is, inertial) effects this ratio is 1. As we will see, however, dynamic effects can either increase or decrease the magnitude of F . Note that Eq. 6a can be rearranged as

$$F = \frac{x_m}{(W/k)}, \quad (6b)$$

where W/k is the deflection that the system would experience if the peak external force were to be applied as a static load. Thus, for this simple model F may be thought of as either a ratio of forces or a ratio of deflections—the two are equivalent.

The second variable is the dimensionless frequency,

$$f = \frac{\omega}{\sqrt{k/m}}, \quad (7)$$

a ratio of frequencies. $\sqrt{k/m}$ is the natural frequency of the spring mass system (in radians per second), the frequency with which it oscillates in the absence of external forces or damping (Thomson 1993). This variable, then, expresses the ratio of the frequency with which the spring-mass system is being driven by the externally applied force to the natural frequency of the spring-mass system.

The third dimensionless variable is

$$\zeta = \frac{2bu_x}{u_x\sqrt{km}} = \frac{2b}{\sqrt{km}}. \quad (8)$$

Here, bu_x is a measure of the viscous force acting on the system (see Eq. 5) and $u_x\sqrt{km}$ is the maximal inertial force that could be applied when the mass is decelerated by the spring (Thomson 1993). The apparently superfluous factor of 2 is explained below.

The fourth (and last) dimensionless variable needed to describe the behavior of a mass on a spring is $t\sqrt{k/m}/2\pi$, the ratio of time to the natural period of the system. This variable is needed to describe when a given force is imposed on the spring. For our purposes, we care only about the magnitude of the maximal force and do not need to know precisely when it occurs. We therefore do not use this final variable.

The dimensionless variables f and ζ can be used to describe F (Thomson 1993):

$$F = \frac{1}{\sqrt{(1-f^2)^2 + (2\zeta f)^2}}. \quad (9)$$

That is, F (the ratio of the actual maximum spring force to the amplitude of the externally applied force) is a function solely of the dimensionless frequency and the ratio of viscous to inertial forces. This relationship is presented in Fig. 2.

For dimensionless frequencies substantially <1 , the force exerted on the mass by the spring is very nearly the same as that imposed by the external force (i.e. $F \cong 1$). In these cases, the mass is being driven at a frequency well below its natural frequency, and the force applied by the spring has time to come to equilibrium with the externally applied force. At dimensionless frequencies $\gg 1$, the force exerted on the mass by the spring is less than that externally imposed. In these cases, the external force does work primarily on the inertia of the mass rather than on the spring. If the frequency of the external driving force is near the natural frequency of the system, however, resonance results, during which the amplitude of motion increases. In the absence of damping, a spring-mass system driven at its resonant fre-

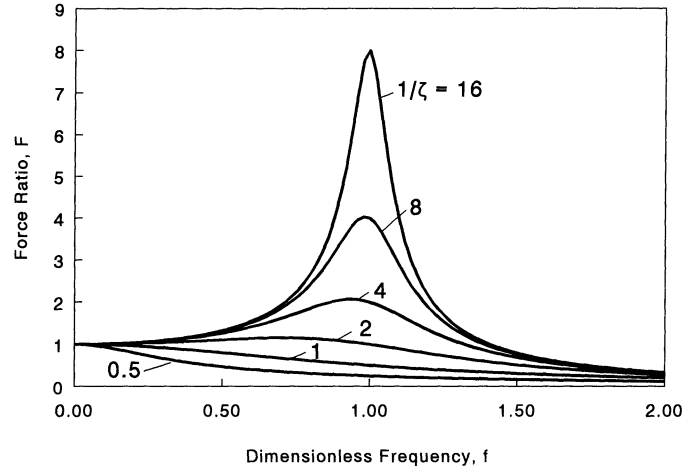


Fig. 2. The dynamic behavior of model 1.

quency gains energy with every cycle of force imposition and tends toward an infinite deflection. By draining energy from the system, damping limits this growth in deflection and therefore controls the force applied by the spring when f is near 1. The more highly damped the system (the larger the value of ζ), the smaller the resulting force. The extra factor of 2 noted previously in Eq. 8 is included so that ζ equals 1 when the system is critically damped (see Thomson [1993] for a discussion of critical damping).

Model 2: A spring-mass system with hydrodynamic forcing

The simple damped spring-mass system described above assumes that the external force is applied directly to the system and is not affected by the system's motion, an assumption that is not at all realistic for many flexible plants and animals. For example, the fluid environment applies an external force to an organism through the imposition of fluid-dynamic forces, and (as we have seen above in Eq. 1 and 3) these forces can be strongly affected by the relative motion of the organism and the fluid. It is thus useful to explore a second simple model of a spring and mass (Fig. 1B). This model differs from the first in two respects. First, the mass is coupled to the fluid environment by drag. Second, we assume that the internal damping of the spring is negligible compared to hydrodynamic damping. In this fashion, drag provides both the external force that drives the system as well as the damping of the system as the mass moves relative to the fluid. The resulting equation of motion is

$$m\left(\frac{d^2x}{dt^2}\right) + kx = K_D u_{x,r} |u_{x,r}|, \quad (10)$$

where (in accordance with Eq. 1)

$$K_D = (1/2)\rho AC_d. \quad (11)$$

For this system, we prescribe the fluid's velocity as

$$u_x = u_{x,m} \sin \omega t, \quad (12)$$

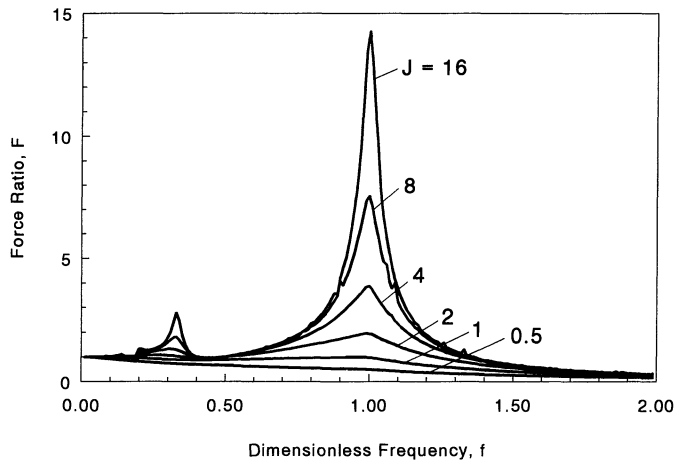


Fig. 3. The dynamic behavior of model 2.

where $u_{x,m}$ is the maximal horizontal velocity of the fluid relative to the substratum.

The dynamics of this system again depend on F and f , as well as on a new dimensionless index (analogous to the inverse of ζ) that we call the *jerk number*, J :

$$J = \frac{u_{x,m} \sqrt{km}}{K_D u_{x,m}^2} = \frac{\sqrt{km}}{K_D u_{x,m}}. \quad (13)$$

The jerk number is the ratio between the maximal inertial force that could act on the moving system (calculated as for the simple spring-mass system) and the maximal hydrodynamic force that a stationary object could encounter (in this case, drag = $K_D u_{x,m}^2$).

Eq. 10 is solved using a 4th-order Runge-Kutta algorithm with an adaptive time step (Press et al. 1992) and the resulting dynamic behavior of this system is shown in Fig. 3. In many respects it is similar to that of model 1. The peak value of F is attained at f equal to 1, and for large jerk numbers this force ratio can be substantially in excess of 1. F decreases with increasing frequency above the resonant frequency, and is < 1 at dimensionless frequencies $\gg 1$.

In this model, the system is damped by drag as the mass moves relative to the surrounding fluid, and, as with the internally damped spring-mass system, the amount of damping sets the maximal F attained when the external forcing is applied at the resonant frequency. Because the damping term (drag) is in the denominator of the jerk number, this means that the smaller the damping the higher the jerk number and the larger the actual force exerted on the mass by the spring.

The principal difference between model 2 and model 1 is the presence of a secondary peak in F at low f (~ 0.3). At these low frequencies, the forces on the mass due to drag and the stretching of the spring have time to approach equilibrium before the direction of the flow changes. There is, however, a tendency for the mass to oscillate resonantly about this "equilibrium" position. This secondary peak in F is due to the inertial forces associated with this oscillation, which at high jerk numbers can lead to inertial forces that are more than twice the externally applied hydrodynamic force.

Model 3: A mass on a discontinuous spring

Although it neglects several forces that potentially may be important (see "real-world examples" below), the model of a spring-mass coupled to the fluid environment by drag (model 2) can serve as a reasonable first approximation for many wave-swept organisms (e.g. anemones, mussels, and stipitate kelps). There are, however, a variety of organisms that are sufficiently flexible such that this model cannot apply, even approximately. For example, an alga such as the feather boa kelp, *Egregia menziesii*, is so flexible that small lateral deflections of the blade result in negligible restoring force, and the blade is thus free to move unimpeded through a wide range of motion. Not until the blade is fully extended in one direction does further deflection result in an elastic restoring force. For organisms such as this, a third simple model is required (Fig. 1C).

The essential difference between this and the preceding model is the inclusion of a discontinuous spring. The effect of this discontinuity can be visualized by thinking of a mass tethered by the combination of a massless spring in series with a massless chain. When taut, the spring-chain has the properties of an elastic spring, and the interaction between the system's mass and the spring-chain are the same as outlined above for the spring-mass system of model 2. Unlike a simple spring, however, the spring-chain can be slack over a range of displacements of the mass. Specifically, if the spring-chain has unstretched length L and is fixed at the origin, the chain is slack as long as the absolute value of the location of the mass is less than L . We assume that when the chain is slack, it exerts no force on the mass. The equation of motion for this system is

$$m \left(\frac{d^2x}{dt^2} \right) + k(\Delta x) = K_D u_{x,r} |u_{x,r}|, \quad (14)$$

where $\Delta x = (L - x)$ when $x > L$, $\Delta x = (-L - x)$ when $x < -L$, and $\Delta x = 0$ otherwise.

As in model 2, the velocity of the fluid (u_x) is sinusoidal along the x -axis with amplitude $u_{x,m}$ and radian frequency ω . The motion of the water is coupled to that of the mass through the imposition of drag, and the stiffness of the taut spring-chain is k .

This model possess one additional dimensionless variable, the *period parameter*, defined as

$$P = \frac{2\pi u_{x,m}}{L\sqrt{k/m}}. \quad (15)$$

This parameter is proportional to the ratio between the distance traveled by the fluid in the natural period of the spring-mass system and the length of the structure. The natural period of the spring-mass system is $2\pi/\sqrt{k/m}$, and we multiply this value by $u_{x,m}$ as an index of the distance traveled by the fluid. Dividing this product by L yields Eq. 15.

The role of P in determining the system's motion can be explained as follows. If the flow imposed on a flexible organism is oscillatory (as it will be in many wave-induced flows), fluid flows only so far in one direction before reversing. If the effective length of an organism is equal to or greater than this maximal fluid travel, the organism can

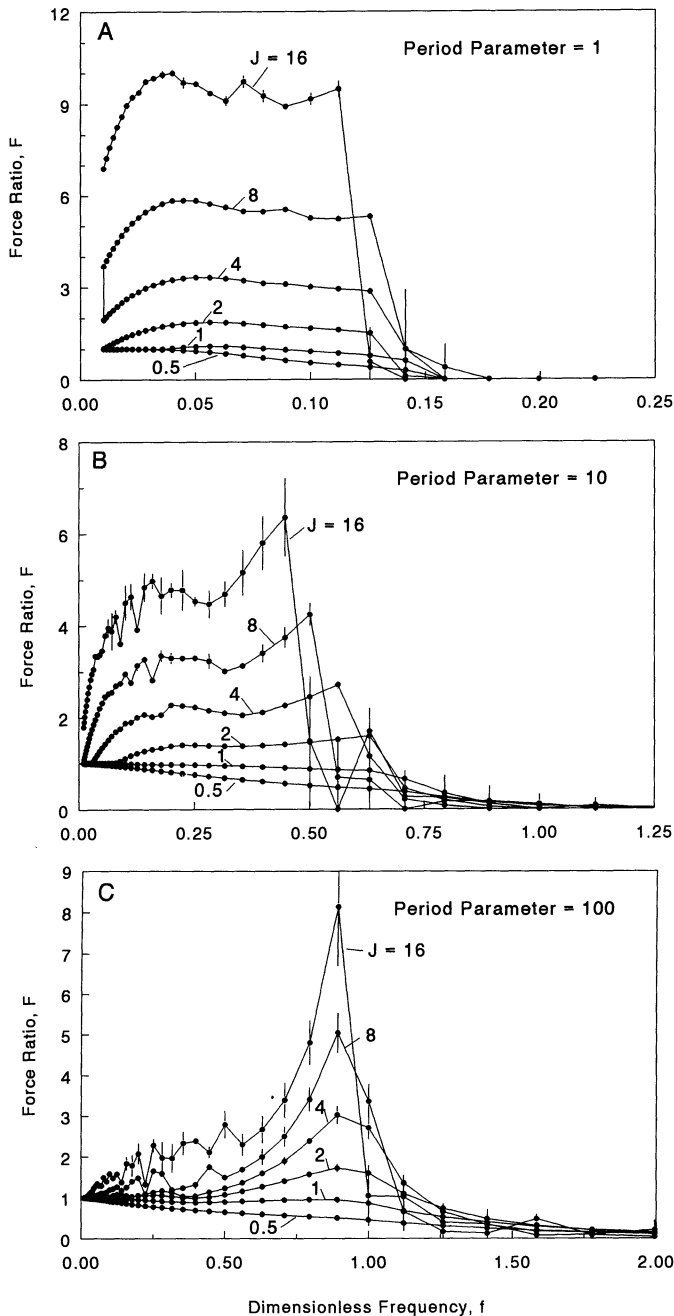


Fig. 4. The dynamic behavior of model 3.

move freely with the flow through its entire cycle, and the necessity of deceleration by the support structure (and thereby of inertial force imposition) is avoided. On the other hand, if the organism substantially stretches its tether before the flow changes direction, an inertial force can be applied as the organism is decelerated.

The results of this model (again obtained using a Runge-Kutta algorithm) are shown in Fig. 4, from which four messages emerge. First, in general and as before, the higher the jerk number, the larger the ensuing F . In this case the ratio of forces can be >10 in some situations. This large ratio is due to the fact that the discontinuous spring, when slack,

does not impede the motion of the mass, and the mass can therefore attain a higher velocity (and momentum) than it would if tethered by a simple spring.

Second, the peak inertial force generally occurs at a dimensionless frequency of <1 , i.e. when the system is being driven below its natural frequency. Consider what is involved in “resonance” for this system. When the mass comes to the end of its tether it is decelerated by the spring-chain and the spring is stretched. After the mass is brought to a halt, it is reaccelerated back from where it came by the energy stored in the spring. This sequence of deceleration–reacceleration occurs at a frequency governed by the natural frequency of the spring-mass system. After being fully reaccelerated by the spring, however, the mass must travel twice the length of the spring-chain before it is again decelerated. Thus, the travel time between deceleration events must be included in the overall period of the resonant oscillation. Because the period of the oscillation is therefore longer than the natural period of the spring-mass system, the resonant frequency is less. Higher jerk numbers are associated with lower maximal fluid velocities (Eq. 13) and with a longer transit time between decelerations. As a general consequence, the higher the jerk number, the lower the frequency at which the peak force ratio is attained.

Third, both the period parameter and the dimensionless frequency affect the conditions under which the spring is in tension. For example, at a period parameter of 1, the spring is placed in tension at some point during a cycle only if the dimensionless frequency is <0.15 . In contrast, at a period parameter of 100, the spring can be in tension at a dimensionless frequency >1.0 . The shift in F with a change in f can be abrupt—below a critical dimensionless frequency, the ratio of inertial to hydrodynamic forces is large; above the critical dimensionless frequency, this ratio is small or zero.

The fourth (and final) message concerns the predictability of the forces acting on the system. For many of the combinations of period parameter, dimensionless frequency, and jerk number shown in this example (Fig. 4), the spring-chain-mass system exhibits dynamically chaotic behavior. The presence of chaos is exemplified by the fact that the maximal force recorded in one cycle of velocity differs from that in the next cycle in an unpredictable fashion, and is indicated here by the error bars in Fig. 4 that show the standard deviation of maximal forces.

The presence of chaotic behavior in this system is not surprising; the discontinuity in the stiffness of the spring-chain provides the nonlinear behavior required for chaos (Moon 1992). For example, the precise timing of the rapid deceleration in one cycle of velocity can, to a large extent, determine the behavior of the system in the subsequent cycle. This makes the system exquisitely sensitive to its instantaneous conditions, a prerequisite for chaotic dynamics.

In summary, a simple model that includes a discontinuous spring (and thereby the potential for a mass to move freely with the flow) results in forces that generally fall into two categories. Within certain ranges of dimensionless frequency and period parameter, the mass never reaches the end of its tether, and the spring-chain is never placed in tension. Outside of this range, however, the ratio of actual to external force is likely to be substantially higher than for a simple

spring-mass system. Owing primarily to the discontinuity in the stiffness of the system, its motions can be chaotic and therefore difficult to predict with any precision.

Models 2 and 3 provide a useful framework for a priori estimation of the importance of inertial loading in wave-swept plants and animals. If one knows the mass, size, and shape of an organism, the period and peak velocity of the flow to which it is exposed, and the stiffness of the organism's support structure, one can calculate the dimensionless frequency, the period parameter, and the jerk number for the organism. Reference to Fig. 3 or 4 will then reveal a first cut estimate of the ratio of actual to maximal drag forces (i.e. F). If the estimated F is large, inertial forces possibly dominate the force imposed on the organism, and going with the flow may not be a viable strategy. If F is small, flexibility is likely to result in diminution of the force experienced by the plant or animal.

Real-world examples

We now turn our attention to wave-swept organisms to explore how the principles explained above can be applied to three specific biological cases. Although by no means exact, these models include several aspects of added complexity that often accompany biological systems: the effects of virtual buoyancy and hydrodynamic added mass, nonlinearity in the system's restoring force, additional freedom of motion not allowed by one-dimensional models, and viscoelastic behavior in the object's supporting structure.

Stipitate kelps—*Eisenia arborea* (Fig. 5A) and *Pterygophora californica* are subtidal kelps of the order Laminariales that often grow in dense understory groves beneath a surface canopy of the giant kelp, *Macrocystis pyrifera* (Abbott and Hollenberg 1974). These seaweeds are large, upright algae that bear their blades at the tips of vertically oriented, sturdy stipes. As such, they grow much like underwater trees. These species typically live in protected to moderately exposed locations at depths ranging from 3 to 20 m, and produce stipes that may reach 2 m in length, with blades extending another 2 m from the stipe's terminus. Both species support approximately equal amounts of blade material for a given stipe length, but of the two, *Eisenia* produces stipes of a much more flexible construction, with elastic moduli about a quarter to a fifth of those of *Pterygophora*. Tensile modulus values, although a function of plant size, are on the order of 50 and 200 MPa, respectively (Gaylord 1997).

As ocean waves pass over these plants, drag action on the blades induces substantial lateral swaying of both the stipe and blades, with the result that the plant may attain considerable momentum. The dynamics of the system are thus analogous to that of model 2, except that for the kelps the bending stiffness of their stipes (rather than a conventional spring) provides the restoring force. The dynamics of these kelps are modeled as follows.

For simplicity, the stipe is treated as a vertical cantilever with the entire effective mass of the system positioned at the free end of the stipe. The effective mass is composed of three parts: the plant's blade mass, the equivalent mass of the stipe

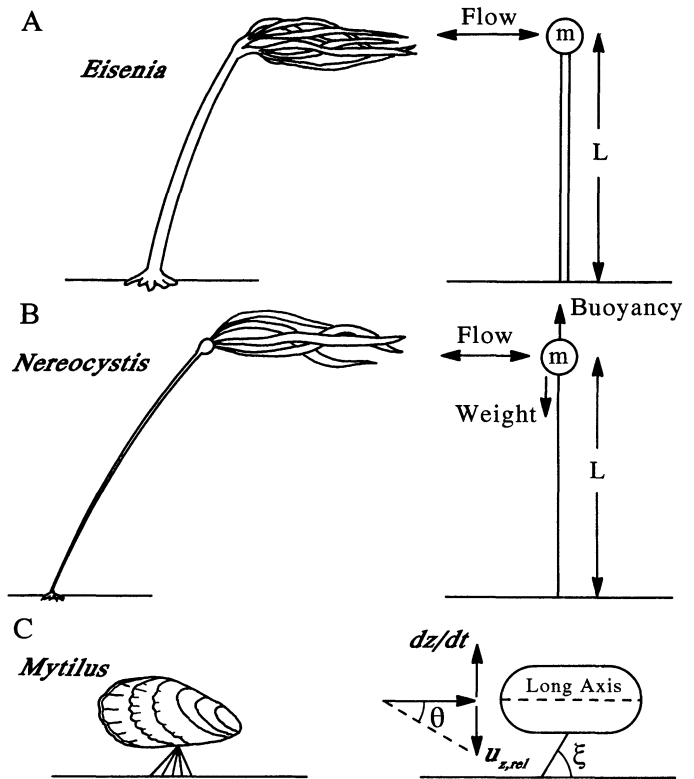


Fig. 5. Biological models. The actual structure of the organism is shown in the column on the left; its model is on the right.

(the mass acting at the end of a massless stipe that behaves as the dynamic equivalent of the distributed stipe mass [Thomson 1993]), and the hydrodynamic added mass of the entire plant, $\rho C_a V$. Here, V is the volume of water displaced by the plant, and C_a is the dimensionless added mass coefficient, a function of the plant's shape. The added mass results from a mass of fluid that behaves, in an inertial sense, as if it tracks the movement of the plant (see Daniel [1984] or Denny and Gaylord [1996] for more on this hydrodynamic effect). For continuity with the other models presented here, the sum of blade mass and equivalent stipe mass of the stipitate kelp is denoted by the variable m ; thus, the overall effective mass in this case is $(m + \rho C_a V)$.

As hydrodynamic forces (primarily drag acting on the blades) deflect the stipe, the stipe's stiffness resists further motion. For small deflections of the stipe tip (less than a tenth of the stipe's length), the spring constant of the system is well approximated by

$$k_{\text{approx}} \cong \frac{3(EI)_{\text{eff}}}{L^3}, \quad (16)$$

where $(EI)_{\text{eff}}$ is the effective flexural stiffness of the stipe, and L is the stipe length (Gere and Timoshenko 1990). If only small deflections occurred, this constant stiffness would mean that stipitate kelps would behave exactly as predicted by model 2. In reality, however, these plants often experience large deflections, and a more general expression must be used for their restoring force. Accordingly, we use large de-

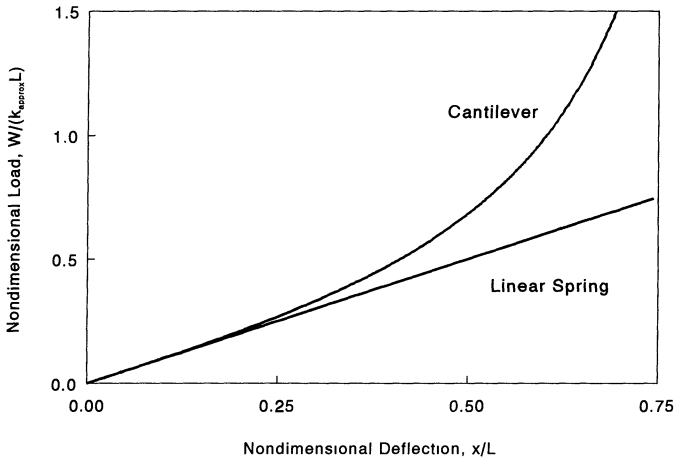


Fig. 6. Stiffness of beams at large deflections that deviate from that of a linear spring.

flexion beam theory (Gere and Timoshenko 1990) where stiffness in the x direction is

$$k = [G(p) - G(p, \Phi)]^2 \frac{(EI)_{\text{eff}}}{L^3}. \quad (17)$$

$G(p)$ and $G(p, \Phi)$ are complete and incomplete elliptic integrals of the first kind, respectively, where p is the elliptic integral's modulus and Φ is the elliptic integral's amplitude (Abramowitz and Stegun 1965), terms related to the instantaneous deflection of the stipe tip. This results in a spring constant that increases with the magnitude of the applied horizontal force. The deviation of the actual stiffness from k_{approx} is shown in Fig. 6.

The simple velocity function of Eq. 12 assumes that the velocity of the water is everywhere the same. Under ocean waves, however, velocity varies through the water column, and to account for this variation Eq. 12 is replaced with a more realistic flow field described by linear wave theory. This theory accounts for effects of wave height and period, water depth, and the distance of an organism's blade mass above the substratum (Kinsman 1965; Denny 1988).

Owing to the ability of kelp blades to reorient in flow, their drag coefficients decline with increasing flow speed. This effect is incorporated via a modification of Eq. 1:

$$\text{Drag} = K'_D u_{x,r} |u_{x,r}|^{\gamma-1} \quad (18)$$

with $\gamma < 2$. Here, $K'_D = (1/2)\rho A S_d$, where S_d is the shape coefficient of drag (see Gaylord et al. 1994). S_d and γ are measured values that equal 0.041 and 1.55 for *Eisenia* and 0.042 and 1.23 for *Pterygophora* (Gaylord 1997).

For completeness, two additional hydrodynamic forces associated with the water's acceleration are also included in the model. The *virtual buoyancy*, $\rho V a_x$, is the force induced by the lateral pressure gradient that causes the water to accelerate. Here $a_x = Du_x/Dt = [(\partial u_x/\partial t) + u_x(\partial u_x/\partial x) + u_z(\partial u_x/\partial z)]$. For stipitate kelps (which live near the solid substratum) the vertical velocities are small. As a consequence, $u_z(\partial u_x/\partial z)$ is small relative to the other terms and is neglected. The second additional force, the *added mass force*, is associated with the acceleration of the fluid relative to the object,

Table 1. Morphological parameters of *Eisenia* and *Pterygophora* with $L = 2$ m.

<i>Eisenia</i>	
Total effective mass, m	3.611 kg
Blade volume, V	$9.923 \times 10^{-4} \text{ m}^3$
Blade area, A	1.112 m^2
Effective flexural stiffness, $(EI)_{\text{eff}}$	14.033 N m^2
<i>Pterygophora</i>	
Total effective mass, m	4.669 kg
Blade volume, V	$1.505 \times 10^{-3} \text{ m}^3$
Blade area, A	1.719 m^2
Effective flexural stiffness, $(EI)_{\text{eff}}$	29.403 N m^2

$\rho C_a V a_{x,r}$, where $a_{x,r} = (Du_x/Dt) - (d^2x/dt^2)$. The added mass force represents the effect of the solid object on the changing pattern of flow in the accelerating fluid around it (Batchelor 1967). An empirically measured value of 1.77 is used for the added mass coefficient, C_a (Gaylord 1997). Because the accelerations under nonbreaking waves are relatively small, these forces constitute only a small portion of the overall hydrodynamic load. Note that the added mass force as defined here is a simplification that neglects terms that are large only for strongly nonuniform (i.e. highly sheared or rotational) flows (see Miloh 1994 for a discussion). The flows under unbroken ocean waves are approximately irrotational and only weakly nonuniform.

The full equation of motion is given by

$$m \frac{d^2x}{dt^2} + kx = K'_D u_{x,r} |u_{x,r}|^{\gamma-1} + \rho V a_x + \rho C_a V a_{x,r}. \quad (19)$$

A rearrangement of this equation illustrates the origin of the effective mass ($m + \rho C_a V$) described earlier:

$$(m + \rho C_a V) \frac{d^2x}{dt^2} + kx = K'_D u_{x,r} |u_{x,r}|^{\gamma-1} + (\rho V + \rho V C_a) a_x. \quad (20)$$

The equation of motion is solved using a 4th-order Runge-Kutta algorithm coupled with interpolation from an elliptic integral look-up table stored in memory. In these equations, x is the horizontal displacement of the stipe tip, and kx is the restoring spring force, with k defined as in Eq. 17. The left-hand side of Eq. 20 represents the sum of system inertia and elastic restoring force, while the right-hand side represents external force contributions from drag and hydrodynamic accelerational forces, respectively.

In this model, the stipe geometry (which in conjunction with the elastic moduli and degree of deflection determines the stiffness), blade area, and plant mass are set by the allometric growth patterns exhibited by each species. Values of these parameters for *Eisenia* and *Pterygophora* plants with a stipe length of 2 m are given in Table 1. Because of this prescribed morphology, a plant of a given stipe length has a fixed $(EI)_{\text{eff}}$, m , and K'_D .

An additional limitation on the model is set by the physics of ocean waves. As waves move into shallow water (where they interact with plants such as *Eisenia* and *Pterygophora*) their height increases and their wave length decreases. At

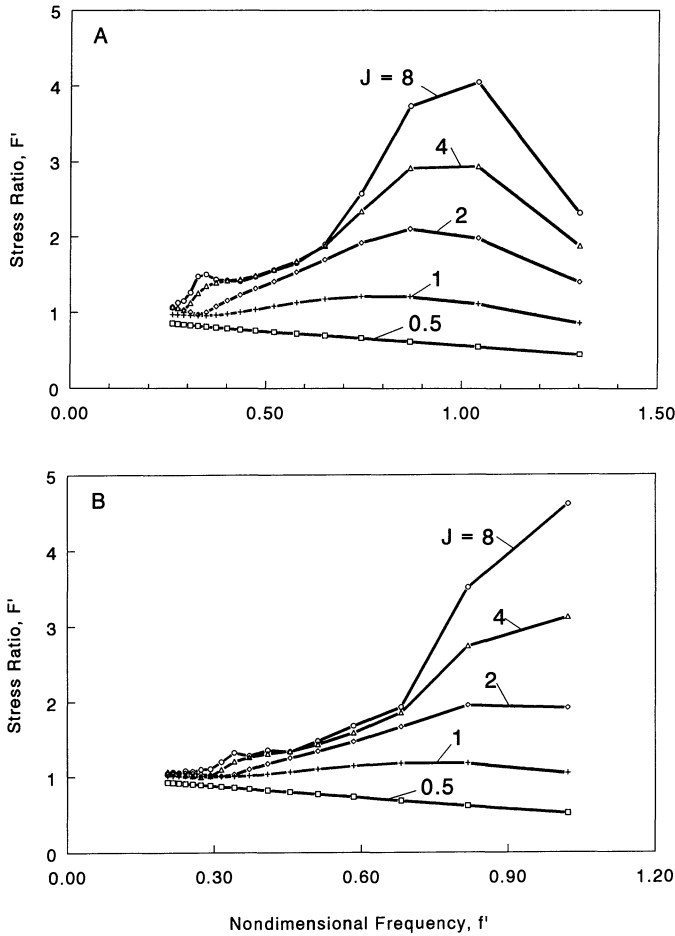


Fig. 7. The dynamic behavior of (A) *Eisenia* and (B) *Pterygophora*.

some point (a wave height $\cong 80\%$ of the water column's depth), this increase in wave steepness causes an instability in the waveform, and the wave breaks. Wave breaking thus sets an upper limit to wave height, which in turn sets an upper limit to the water velocity that can be imposed on seaweeds. These restrictions in morphology and water velocity mean that only a portion of the parameter space shown in Fig. 3 can actually be experienced by any plant. In particular, this constraint sets a lower limit on the jerk number that can be experienced by a plant of given size growing at a given depth and exposed to waves of a given period. Wave periods of 1–20 s are used, spanning the range typical of nearshore ocean waves. Note that for this model k_{approx} (rather than k , which varies through time as the plant sways) is used to calculate J and f .

The model is initiated with x of 0. A continuous traveling waveform of fixed amplitude and period is then allowed to move the water, and the plant responds. The deflection of the stipe is recorded at each time step, and the maximal deflection in each wave cycle is noted. This procedure is then repeated for different wave periods.

Unlike models 1–3, in which the force acting on the system is linearly related to the deflection of a simple spring, the deflection of a cantilever-like algal stipe is not linearly

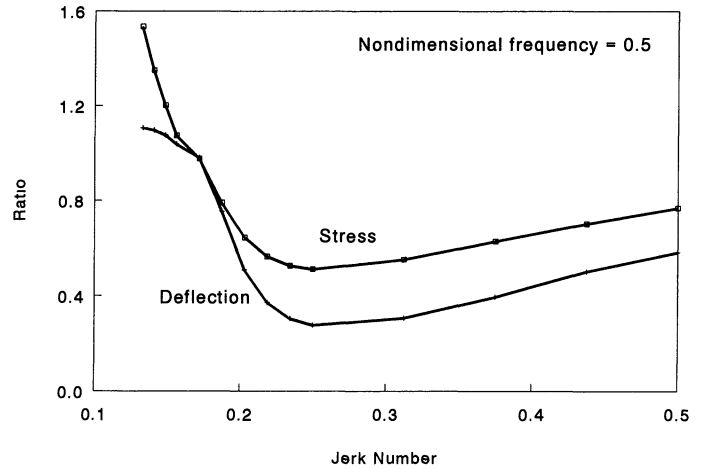


Fig. 8. The dynamic behavior of stress and deflection in *Pterygophora* as a function of jerk number. At low J , the nonlinear stiffness of the cantilever plays an important role in the system's dynamics.

related to force (Fig. 6). Furthermore, the bending force applied to the stipe is not linearly related to the stress (force per area) imposed on the stipe's material. Ultimately it is this stress that is of biological interest because it determines whether the stipe's material will break. Thus, in this case we use an alternative to F , where F (as defined previously) is the ratio of forces or, equivalently, deformations. This alternative, F' , is the ratio of the actual maximal stress to the stress that would be imposed by drag in a steady flow with velocity $u_{x,m}$.

Figure 7 shows typical examples of the stress ratios that result from the movement of waves past *Eisenia* and *Pterygophora* individuals. The similarity of this relationship to that of model 2 is striking. Just as in Fig. 3, both panels of Fig. 7 show elevated peaks near a nondimensionalized frequency of 1. For the jerk numbers shown, higher maximum stresses occur at larger jerk numbers, and at a jerk number of 0.5 the stress ratio is < 1 across the full range of nondimensionalized frequency. The presence of a secondary peak at f of ~ 0.3 is also apparent. Although these graphs show data from only 2 m -tall plants growing in 5 m of water, results are qualitatively identical across both depth and plant size.

This simple picture can be affected, however, by the nonlinear stiffness characteristic of the stipes of these cantilever-like kelps. This effect is seen in Fig. 8, which displays data for both relative deflection and relative stress as a function of jerk number at a fixed nondimensional frequency. At this f , both deflection and stress ratios increase monotonically with increasing jerk number for $J > 0.25$. When J is very low, however, wave heights are large, flows are rapid, and the plants are bent to large deflections where their nonlinear behavior becomes important. The net result is that the ratios of dynamic to static deflection and stress increase with decreasing jerk number for $J < 0.25$. These nonintuitive results (peculiar to structures with nonlinear stiffness) demonstrate that care must be taken when generalizing from any simple model to more complicated flow-organism scenarios.

The bull kelp, *Nereocystis leutkeana*—*Nereocystis* comprises a holdfast, a thin, flexible, ropelike stipe terminated by a float (the pneumatocyst), and a mass of fronds (Fig. 5B). This species is characteristically found on fully exposed, wave-swept shores from central California to Alaska, although it may be locally abundant in more protected sites (e.g. Puget Sound). The plant grows in water depths from 5 to ~20 m (Abbott and Hollenberg 1978).

The ropelike stipe of *Nereocystis* is constructed from an extensible, reasonably elastic material with a modulus of $\sim 10^7$ Pa (Koehl and Wainwright 1977; Johnson and Koehl 1994). In this respect, the stipe is capable of performing as the type of spring-chain structure used in model 3. The preponderance of the plant's mass is concentrated at the distal end of the stipe in the frond and pneumatocyst, and it is upon these structures that flowing water interacts with the plant, largely through the imposition of drag (Koehl and Wainwright 1977; Johnson and Koehl 1994).

The morphology of *Nereocystis* is thus reminiscent of model 3. The primary difference between the kelp and model 3 is the presence in the kelp of the buoyant pneumatocyst. The action of this float is to pull upward on the stipe, while the action of drag is (in large part) to pull horizontally. Thus, the motion of the plant is necessarily two dimensional in contrast to the one-dimensional models presented so far.

The dynamics of *Nereocystis* are modeled in a fashion similar to that of Friedland and Denny (1995) and Utter and Denny (1996). We treat the frond, stipe, and pneumatocyst masses as a combined mass concentrated at the end of a massless spring-chain of unstretched length L . The mass is tethered to the origin ($x = 0, z = 0$) by the stipe. When the radial distance from the origin to the concentrated mass is less than L , the stipe is assumed to exert no tension on the mass. Once stretched taut, however, the stipe exerts a tension proportional to its deformation, and this tension acts along the line connecting the mass and the origin.

The equations of motion are

$$(m + \rho C_a V) \frac{d^2 x}{dt^2} + k_x \Delta L = K'_D u_{x,r} (u_{x,r}^2 + u_{z,r}^2)^{(\gamma-1)/2} + (\rho V + \rho C_a V) a_x \quad (21)$$

$$(m + \rho C_a V) \frac{d^2 z}{dt^2} + k_z \Delta L = K'_D u_{z,r} (u_{x,r}^2 + u_{z,r}^2)^{(\gamma-1)/2} + (\rho V + \rho C_a V) a_z + \rho g V - mg. \quad (22)$$

Water velocities are again calculated using linear wave theory. The mass of the plant, its hydrostatic buoyancy ($\rho g V$), weight (mg), maximal projected area, and stipe cross-sectional area are all taken to be allometric functions of stipe length as shown in Table 2. The accelerational force acting on the mass is calculated as described above for cantilever-like algae, and an added mass coefficient C_a of 3.0 is used (Utter and Denny 1996). By analogy to $u_{x,r}$, $u_{z,r}$ is the vertical water velocity relative to the point element and the vertical acceleration of fluid, $a_z = [(\partial u_z / \partial t) + u_z (\partial u_z / \partial z) + u_x (\partial u_x / \partial x)]$. Measurements made by Johnson and Koehl (1994) sug-

Table 2. Morphological parameters of *Nereocystis* with $L = 8$ m.

Mass, m	2.24 kg
Blade area, A	1.96 m ²
Stipe cross-sectional area, A_{xs}	1.32×10^{-4} m ²
Net buoyancy	10.29 N
Volume, V	2.2×10^{-3} m ³
Elastic modulus, E	1.2×10^7 N m ⁻²

gest that S_d is 0.016 for this plant, and measurements made by Utter and Denny (1996) suggest that γ equals 1.6.

The extension of the stipe, ΔL , is $(\sqrt{x^2 + z^2} - L)$ when the stipe is stretched beyond its resting length L , and ΔL equals 0 otherwise. In these equations, k_x and k_z are the horizontal and vertical components of the stiffness of the plant's stipe:

$$k_x = k \cos[\tan^{-1}(z/x)], \quad (23)$$

$$k_z = k \sin[\tan^{-1}(z/x)]. \quad (24)$$

The intrinsic stiffness of the stipe, k , is calculated from its cross-sectional area A_{xs} , length L , and elastic modulus E :

$$k = \frac{EA_{xs}}{L}. \quad (25)$$

For a stipe 8 m long and a material stiffness, E , of 1.2×10^7 Pa, k is 1.97×10^2 Nm⁻¹. The natural frequency of the spring-mass system (mass of 2.24 kg) is 9.4 rad s⁻¹.

These equations are solved using a 4th-order Runge-Kutta algorithm with an adaptive time step (Press et al. 1992). Wave periods from 1 to 20 s are used. For each period, the amplitude of the water wave is adjusted to give a specified value of the jerk number. In this fashion, once the length of a plant has been chosen, the calculations provide a measure of F as a function of nondimensional frequency, jerk number, and period parameter. The use of F here (rather than F') is appropriate because the stipe of *Nereocystis* is loaded in tension rather than bending, so (given the assumption of constant E) the stress in the stipe's material is linearly related to both deflection and force.

The calculation begins with the plant stationary and extended to its unstretched length vertically above the origin. A continuous sinusoidal traveling waveform of fixed amplitude is then allowed to move the water, and the plant responds. The tension in the stipe is recorded at each time step, and the maximal tension in each wave cycle is noted and used to calculate F . The calculation is continued until F is virtually constant (a variation of <0.002 between successive wave cycles).

As with the model of *Eisenia* and *Pterygophora*, the non-dimensional frequency, jerk number, and period parameter of the model of *Nereocystis* are confined to a subset of values that corresponds to the values of stipe length, wave period, and wave height found in the real world. For example, given a stipe length (which sets k , m , and K'_D) and jerk number, the maximum water velocity is fixed (see Eq. 13). Linear wave theory shows that maximum water velocity is in turn a function of wave height, wave period, and water-column depth (Kinsman 1965; Denny 1988). As a result, for a fixed

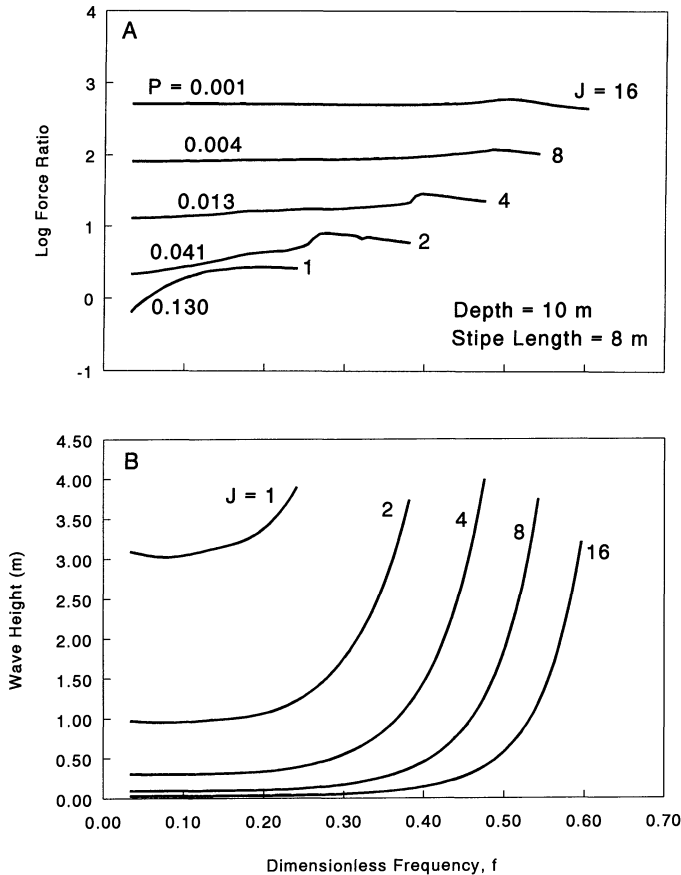


Fig. 9. The dynamic behavior of *Nereocystis*. (A) Force ratio as a function of nondimensional frequency. (B) The wave heights required to maintain a constant jerk number. Linear wave theory shows that wave height is governed by two factors related to wave frequency. One of these decreases linearly with increasing frequency, the other increases exponentially with increasing frequency. For the range of frequencies used here, the second (exponential) term dominates, and wave height at constant jerk number increases with increasing f .

depth, when wave period is varied to change the dimensionless frequency (see Eq. 7), wave height must be adjusted to maintain a constant jerk number—the higher the dimensionless frequency, the higher the waves must be (Fig. 9B). However, as noted previously, there is a physical limit to the height an ocean wave can attain in water of a given depth (Denny 1988). Thus, the breaking characteristics of ocean waves set both the upper limit to dimensionless frequency and the lower limit to the jerk number that kelps such as *Nereocystis* experience.

Note that for a plant of fixed length (and therefore fixed k and m), the period parameter is a function solely of maximum velocity. Because maximum velocity is itself determined by the jerk number, J and P are not independent. In the calculations made here for a fixed value of J , P is allowed to vary, but it is always small (<0.13 for $J = 1$).

Results are shown in Fig. 9A. Although the model of *Nereocystis* is more complex than model 3 in that it is two-dimensional and includes buoyancy and the added mass force, the results are actually simpler and more predictable.

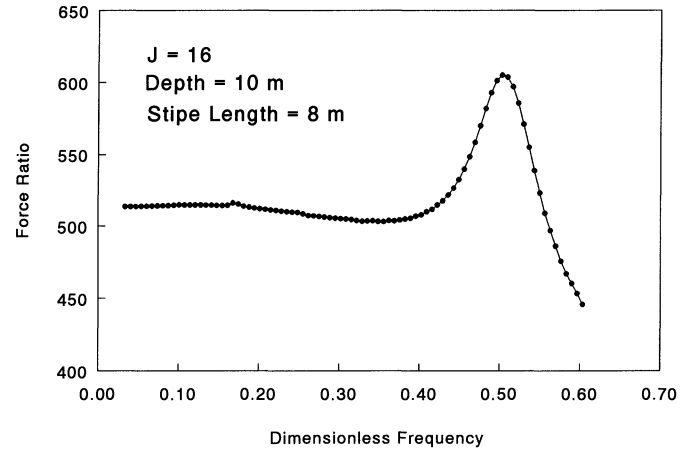


Fig. 10. Data from Fig. 9A replotted on a linear ordinate to show more clearly the peak in force ratio.

The ratio of inertial to hydrodynamic forces increases with an increase in jerk number, and in this case F reaches values >600 (note the logarithmic ordinate in this figure). As with models 1 and 2, F peaks at a certain f (see Fig. 10). In this model, F peaks at dimensionless frequencies varying from ~ 0.2 to 0.5 , depending on the jerk number. Unlike model 3, in which the dimensionless frequency at the maximal F decreased with increasing jerk number, in the two-dimensional case of the bull kelp, f at peak F increases with increasing J .

Much of the simplicity of the bull kelp's behavior in this example is due to the fact that the buoyancy of the plant is sufficient to maintain tension on the stipe throughout the passage of a wave. Thus, the sharp cutoff of inertial force above a certain f characteristic of model 3 is not seen, and the model of *Nereocystis* does not exhibit chaotic dynamics for the parameters used in this example.

The marine mussel, Mytilus—We now examine the dynamics of mussels of the genus *Mytilus*, one of the most common benthic invertebrates in exposed regions of the temperate oceans (Fig. 5C). These mussels are commonly found in beds of conspecifics or congeners, but for simplicity we consider a solitary mussel, for example one within a newly formed patch (sensu Paine and Levin 1981). Unlike our previous examples, the flexible support here has both elastic and viscous behaviors.

Mytilus mussels are attached to the substrate with byssal threads, a system of fibrous strands whose mechanical properties are similar to collagen (Smeathers and Vincent 1979; Vincent 1982). Each byssal thread is attached to a common stem; the stem, in turn, is continuous with a root in the byssal gland which secretes these threads. An average thread is ~ 15 – 20 mm long and is divided into a corrugated portion proximal to the root and a smooth distal portion. The distal portion is anchored to the substratum by an adhesive disk. Mechanical failure can occur in any of these three portions, either as a function of the force per thread (failure within the thread or adhesive disk) or due to the combined force on the system of threads (failure in the common stem; Bell 1996). Significantly, the byssal system includes a byssal retractor muscle that maintains most of the threads in tension

at all times. Muscle tension, therefore, removes any slack from the threads, giving rise to a situation that is substantially different from model 3. Some movement is permitted by the flexibility of the threads, however, and momentum can thus accumulate as the body of the mussel moves. To account for the interactions among momentum, byssus mechanics, and fluid dynamics, we describe a general model of the forces experienced by a mussel subjected to a breaking wave. We then use the model to explore the consequences of flexibility in the support structure to the total force experienced by the mussel's byssus.

Unlike the flow experienced by subtidal kelps (which at any given position oscillates sinusoidally), the flow initially imposed on an intertidal mussel by a breaking wave is characterized by water moving shoreward and generally parallel to the substratum with a velocity that quickly reaches some maximum value. Subsequently, velocity declines and then reverses during seaward flows, but it is the initial rapid increase in flow velocity that is likely to exert the largest force on mussels. We model the initial shoreward component of flow with a simple exponential function that mimics the flows recorded by Denny et al. (1985):

$$u_x = u_{x,m}[1 - \exp(-t^2/\tau)], \quad (26)$$

where $u_{x,m}$ is in this case the asymptotic maximum horizontal water velocity, τ is the time constant for increase in water velocity, and t is time. The derivative of this expression gives the acceleration of the water as it flows shoreward, and u_z is assumed to be zero. Although this expression does not capture the turbulent fluctuations associated with surf-zone flows, and does not take into account any flow perpendicular to the substratum, it does mimic the major features of the flow that determine the total and maximum forces associated with large-scale fluid accelerations.

Note that flow modeled in this fashion is aperiodic, with the consequence that we cannot directly calculate the frequency ω for surf-zone flow, and therefore cannot use Eq. 7 to calculate a dimensionless frequency. We thus define an alternative dimensionless frequency:

$$f' = \frac{2\pi}{\tau \sqrt{\frac{k_1 + k_2}{m}}}, \quad (27)$$

where $k_1 + k_2$ is the maximal spring stiffness of the system (see below).

The equations of motion for *Mytilus* are

$$\begin{aligned} (m + \rho C_a V) \frac{d^2 x}{dt^2} + k_x \Delta L \\ = K_D u_{x,r} \sqrt{u_{x,r}^2 + u_{z,r}^2} + K_L u_{z,r} \sqrt{u_{z,r}^2 + u_{x,r}^2} \\ + (\rho V + \rho C_a V) a_x, \end{aligned} \quad (28)$$

$$\begin{aligned} (m + \rho C_a V) \frac{d^2 z}{dt^2} + k_z \Delta L \\ = K_L u_{x,r} \sqrt{u_{z,r}^2 + u_{x,r}^2} - K_D u_{z,r} \sqrt{u_{z,r}^2 + u_{x,r}^2} \\ + (\rho V + \rho C_a V) a_z + \rho g V - mg. \end{aligned} \quad (29)$$

$K_L (= \frac{1}{2} \rho C_L A)$ is analogous to K_D , and C_l is the dimensionless lift coefficient.

Unlike the flexible kelps (for which the hydrodynamic force coefficients are assumed to be independent of the direction of flow), the coefficients C_d , C_l , and C_a as applied to mussels depend on the vector components of the relative flow in relation to the horizontal, long axis of the animal's shell (Fig. 5C; the animal is assumed not to rotate, although it may translate both horizontally and vertically):

$$C_d = C_{d,par} |\cos(\theta)| + C_{d,perp} |\sin(\theta)| \quad (30)$$

$$C_l = C_{l,par} |\cos(\theta)| \quad (31)$$

$$C_a = C_{a,par} |\cos(\theta)| + C_{a,perp} |\sin(\theta)| \quad (32)$$

$$\theta = \tan^{-1} \left(\frac{dz/dt}{u_{x,r}} \right). \quad (33)$$

Here, the subscripts *par* and *perp* designate flows that are either parallel or perpendicular to the long axis of the shell, respectively. θ is the angle between the relative flow and the long axis of the shell (Fig. 5C), and dz/dt is the vertical velocity of the mussel. Note that because we have assumed that flow in the z direction is zero, $u_{z,r} = -dz/dt$. $C_{l,perp}$ is assumed to be zero.

The externally applied forces on a mussel shell are instantaneously balanced by the byssal thread system. Like most biological structures, the byssus displays viscoelastic properties—the stiffness of the strands is determined not only by the strain of the material (that is, by its relative change in length), but also by the *rate* of strain. We choose a model of a standard linearly viscoelastic solid to describe the response of the byssus to strain, as this model has previously been shown to approximate closely structures resembling collagen (Vincent 1982). This model represents a linear viscoelastic system (e.g. Bell 1996), but incorporates time dependence. The standard linear model consists of two parallel springs (with stiffnesses k_1 and k_2) and a viscous element (a dashpot of viscosity η) in series with the second spring (Fig. 11). The mathematical representation of the tension created in the complete byssus system is thus in the form of a coupled system of differential equations:

$$k_{bys} = n[k_1 \Delta L + k_2 (\Delta L - L_\eta)] \quad (34)$$

$$k_z = k_{bys} \sin(\xi) \quad (35)$$

$$k_x = k_{bys} \cos(\xi) \quad (36)$$

$$\xi = \tan^{-1}[z(t)/x(t)] \quad (37)$$

$$dL_\eta/dt = k_2 (\Delta L - L_\eta)/\eta, \quad (38)$$

where $x(t)$ and $z(t)$ are instantaneous distances from the initial position of the animal, n is the number of byssal threads, and ξ is the angle of the byssus with respect to the horizontal substratum (Fig. 5C). ΔL is defined as for *Nereocystis*. The "length" of the viscous element (L_η) is initially 0 and is subsequently defined implicitly by Eq. 38, which describes the contribution of the dashpot term.

As before, this coupled system of 2nd-order differential equations is solved using a Runge-Kutta method in which the time step is adjusted to obtain suitable levels of accuracy.

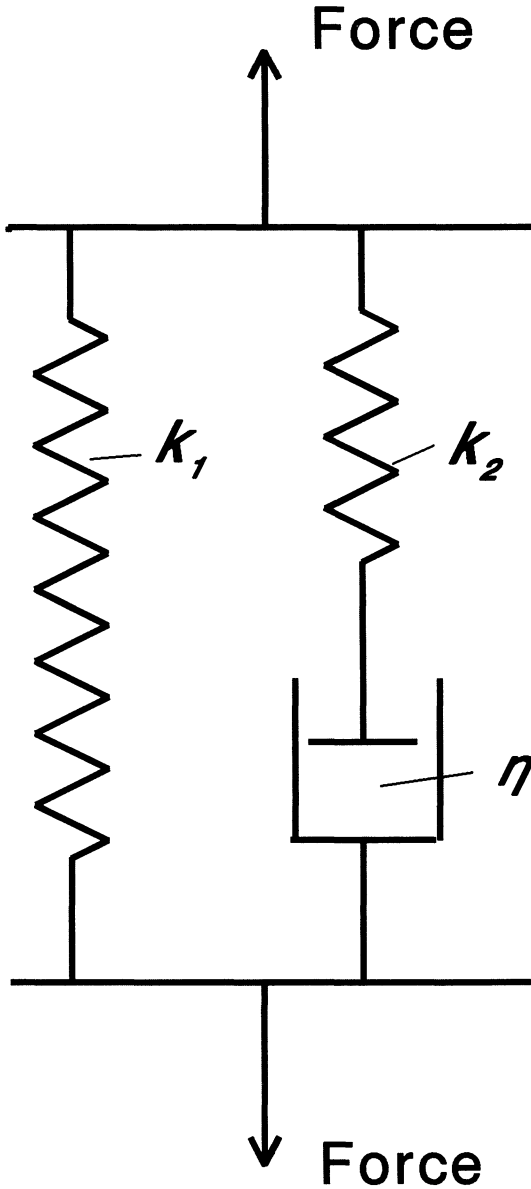


Fig. 11. A schematic diagram of the standard solid used in the mussel model.

Very small time steps (<1 ms) are required in this case because the system of equations is very stiff for the particular parameters used.

To solve the system we begin with a baseline set of parameters that describes body dimensions, water motions, and material properties of the support structures (Table 3). These values are chosen to represent those experienced by a typical 10-cm-long mussel. A maximum water velocity of 7 m s⁻¹ with an acceleration time constant (τ , Eq. 26) ranging from 0.3 to 5 ms was used for this baseline set as it best reflects the wave dynamics shown in Denny et al. (1985). Body dimensions (projected area and volume) were also derived from allometric relationships presented in Denny et al. (1985). Our choice of material properties for byssal threads follows from the measurements of relaxation moduli detailed

Table 3. Morphological parameters of *Mytilus* with $L = 10$ cm.

Supporting structure	
Resting length of byssus, L_{bys}	0.02 m
Number of byssal threads, n	50
Spring constant (series), k_1	16 N m ⁻¹
Spring constant (parallel), k_2	27 N m ⁻¹
Viscous element, η	5460 Pa s
Mussel morphology	
Length, L	0.1 m
Mass, m	0.127 kg
Area,* A	0.004 m ²
Hydrodynamic coefficients	
Drag coefficient (x direction), $C_{d,par}$	0.2
Drag coefficient (z direction), $C_{d,perp}$	0.8
Lift coefficient (x direction), $C_{l,par}$	0.1
Lift coefficient (z direction), $C_{l,perp}$	0.0
Added mass coefficient (x direction), $C_{a,par}$	0.2
Added mass coefficient (z direction), $C_{a,perp}$	1.0

* Maximal surface area of the mussel calculated as $\pi(\text{length}/2)(\text{width}/2)$. Actual differences in area due to the angle of flow are accounted for by adjusting the coefficients of drag and added mass.

in Smeathers and Vincent (1979): $k_1 = 16$ N m⁻¹, $k_2 = 27$ N m⁻¹, $\eta = 5460$ Pa s⁻¹. The number and length of byssal threads are highly variable among individuals and appear to depend upon environmental conditions and size (e.g. Young 1985). For our baseline mussel we use 50 byssal threads of 2-cm length and total cross-sectional area of 0.8 mm².

Note that in this viscoelastic model, the stiffness of the system is itself a function of the system's dynamics. Because the jerk number depends on the stiffness (Eq. 13), this means that J cannot be calculated as before. Instead, we define an alternative jerk number, J_{visc} ,

$$J_{visc} = \frac{\sqrt{(k_1 + k_2)m}}{Ku_{x,m}}, \quad (39)$$

where $(k_1 + k_2)$ is again the maximal stiffness of the structure, $K = \frac{1}{2}\rho\sqrt{C_d^2 + C_l^2} A$, and A is the maximal projected area of the mussel.

The results are shown in Fig. 12, and are again similar to

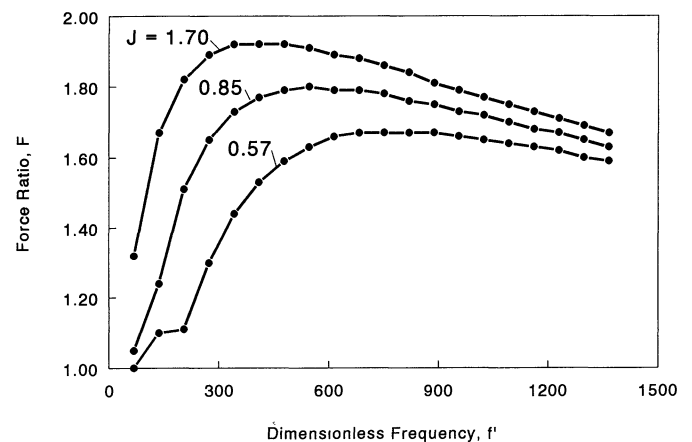


Fig. 12. The dynamic behavior of *Mytilus*.

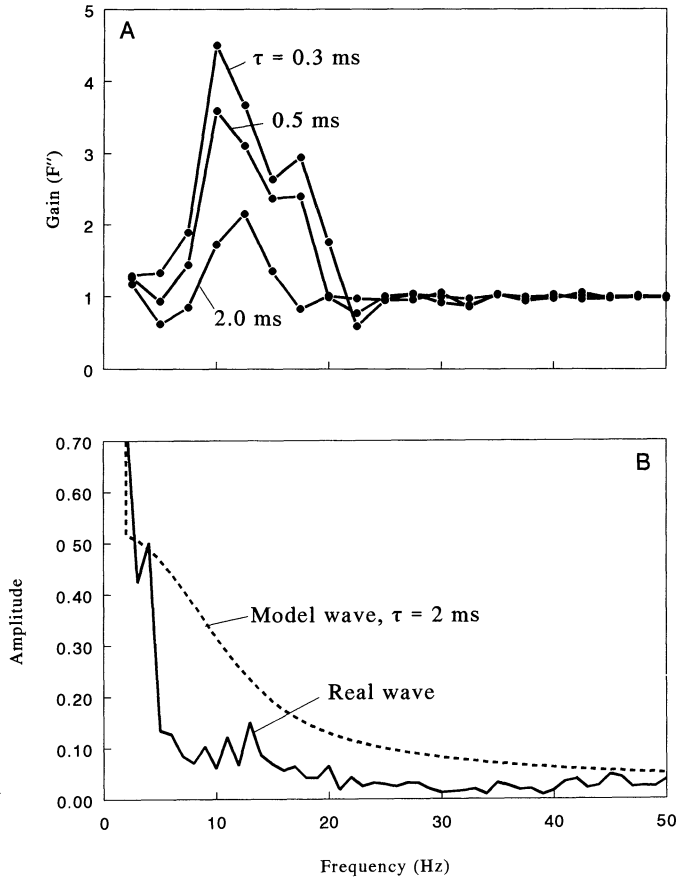


Fig. 13. Fourier analysis of the transfer function between the energy imparted by a wave and the resulting force in a mussel's byssus. (A) Gain (F'') as a function of frequency for a mussel subject to a simple wave function (Eq. 25). (B) Scaled amplitude of the Fourier coefficients of our simple wave model (Eq. 25) and those from an example of a real wave.

those from model 2. The ratio of actual to static forces is maximal at one particular f' , and the higher the jerk number, the higher the force ratio. For the parameter range used here, that peak force is always greater than the maximum force imposed by a steady, unidirectional flow.

In models 1–3 as well as in the models of kelps developed above, flow is characterized by a single frequency ω . In contrast, the flow applied here to a mussel simultaneously contains an entire spectrum of frequencies. Thus, to characterize fully the initial upsurge of a wave in a manner analogous to that of previous models, we can represent the flow as a linear series of sine and cosine terms whose superposition gives the form of the overall wave. In similar fashion, to characterize fully the tension in the byssus, we can represent the instantaneous tension by a superposition of tensions associated with a spectrum of frequencies. In standard engineering practice, this decomposition of the imposed and resulting forces into their frequency components is the role of the transfer function, the ratio of the Fourier transform of an output signal to that of an input signal (Marmarelis and Marmarelis 1978). The transfer function, here given the symbol

F'' , reflects the *gain* of a dynamic system and is analogous to the previously defined ratio of forces, F .

The transfer function of a mussel is shown in Fig. 13A. For the simulated wave used above, frequency-specific F'' is sensitive to the time constant of the wave—the shorter the time constant, the higher the gain in force. Importantly, however, the frequency at which F'' is maximal is largely independent of the wave's time constant of acceleration. Therefore, even though real waves may contain significant energy at frequencies below or above that associated with the maximal F'' (Fig. 13B), it is the energy at frequencies for which F'' is high that has the greatest potential to load the structure substantially.

Note that the mechanical properties of the organism determine precisely where that maximum frequency occurs. Thus, the mechanical properties of the organism's support system can potentially be tuned to reduce inertial forces. Keep in mind, however, that F'' is an index of the ratio of the force actually imposed on the byssus at a given frequency to the force applied externally. Even if this ratio is small, the absolute force applied to the byssus can be large if the externally applied force is sufficiently large.

Note also that the model presented here for the dynamics of mussels in flow, although incorporating many aspects of the actual system, is far from exact. For example, in real mussels byssal threads occur in a range of lengths, are deployed at a range of angles to the substratum, and have a range of preload tension. As a consequence of the simplifications made in our model, the results must be viewed as a ballpark estimate rather than a precise prediction.

Conclusions

Although the interactions of flexible organisms with their fluid surroundings can be complex, the models presented here allow several general conclusions to be drawn: (1) Going with the flow can indeed reduce the total force imposed on an organism, but typically only at low jerk numbers and at dimensionless frequencies well removed from some critical value (generally equal to 1). (2) For high jerk numbers and dimensionless frequencies near the critical value, the inertial force imposed on an organism by its own momentum can substantially increase the overall force. (3) In some (and perhaps many) cases, the size of organisms and the nature of the flows to which they are exposed determine a priori the range of jerk numbers and dimensionless frequencies that will be encountered. The models presented here may therefore provide the basis for useful predictions of the importance of inertial loading in fluid-swept plants and animals. (4) The tendency for inertial loading to peak at specific dimensionless frequencies raises the possibility that the structure of organisms can be tuned (either by evolution or physiological response) to avoid potentially damaging loads.

References

- ABBOTT, I. A., AND G. J. HOLLENBERG. 1976. Marine algae of California. Stanford Univ. Press.
- ABRAMOWITZ, M., AND I. A. STEGUN. 1965. Handbook of mathematical functions. Dover.

- BATCHELOR, G. K. 1967. An introduction to fluid dynamics. Cambridge Univ. Press.
- BELL, E. C. 1996. Mechanical design of mussel byssus: Material yield enhances attachment strength. *J. Exp. Biol.* **199**: 1005–1017.
- CARRINGTON, E. 1990. Drag and dislodgment of an intertidal macroalga: Consequences of morphological variation in *Mastocarpus papillatus* Kützing. *J. Exp. Mar. Biol. Ecol.* **139**: 185–200.
- DANIEL, T. L. 1984. Unsteady aspects of aquatic locomotion. *Am. Zool.* **24**: 121–134.
- DAYTON, P. K. 1971. Competition, disturbance, and community organization: The provision and subsequent utilization of space in a rocky intertidal community. *Ecol. Monogr.* **41**: 351–389.
- DENNY, M. W. 1988. Biology and the mechanics of the wave-swept environment. Princeton Univ. Press.
- . 1993. Disturbance, natural selection, and the prediction of maximal wave-induced forces. *Contemp. Math.* **141**: 65–90.
- . 1994. Roles of hydrodynamics in the study of life on wave-swept shores, p. 169–204. *In* P. C. Wainwright and S. M. Reilly [eds.], *Ecomorphology: Integrative organismal biology*. Univ. Chicago Press.
- . 1995. Predicting physical disturbance: Mechanistic approaches to the study of survivorship on wave-swept shores. *Ecol. Monogr.* **65**: 371–418.
- , T. L. DANIEL, AND M. A. R. KOEHL. 1985. Mechanical limits to size in wave-swept organisms. *Ecol. Monogr.* **55**: 69–102.
- , AND B. P. GAYLORD. 1996. Why the urchin lost its spines: Hydrodynamic forces and survivorship in three echinoids. *J. Exp. Biol.* **199**: 717–729.
- FRIEDLAND, M. T., AND M. W. DENNY. 1995. Surviving hydrodynamic forces in a wave-swept environment: Consequences of morphology in the feather boa kelp *Egregia menziesii* (Turner). *J. Exp. Mar. Biol. Ecol.* **190**: 109–133.
- GAYLORD, B. P. 1997. Effects of wave-induced water motion on nearshore macroalgae. PhD. thesis, Stanford Univ.
- GAYLORD, B., C. BLANCHETTE, AND M. W. DENNY. 1994. Mechanical consequences of size in wave-swept algae. *Ecol. Monogr.* **64**: 287–313.
- GERE, J. M., AND S. P. TIMOSHENKO. 1990. *Mechanics of materials*. 3rd Ed. PWS-Kent Publ.
- JOHNSON, A. S., AND M. A. R. KOEHL. 1994. Maintenance of dynamic strain similarity and environmental stress factor in different flow habitats: Thallus allometry and materials properties of a giant kelp. *J. Exp. Biol.* **195**: 381–410.
- KINSMAN, B. 1965. *Wind waves*. Prentice-Hall.
- KOEHL, M. A. R. 1977a. Effects of sea anemones on the flow forces they encounter. *J. Exp. Biol.* **69**: 87–105.
- . 1977b. Mechanical organization of cantilever-like sessile organisms: Sea anemones. *J. Exp. Biol.* **69**: 127–142.
- , AND S. A. WAINWRIGHT. 1977. Mechanical design of a giant kelp. *Limnol. Oceanogr.* **22**: 1067–1071.
- MARMARELIS, P. Z., AND V. Z. MARMARELIS. 1978. *Analysis of physiological systems: The white noise approach*. Plenum.
- MENGE, B. A. 1978. Predation intensity on a rocky intertidal community: Relation between predator foraging activity and environmental harshness. *Oecologia (Berlin)* **34**: 1–16.
- MILOH, T. 1994. Pressure forces on deformable bodies in non-uniform inviscid flows. *Q. J. Appl. Math.* **47**: 635–661.
- MOON, F. C. 1992. *Chaotic and fractal dynamics*. John Wiley & Sons.
- PAINE, R. T., AND S. A. LEVIN. 1981. Intertidal landscapes: Disturbance and the dynamics of pattern. *Ecol. Monogr.* **51**: 145–178.
- PRESS, H. W., S. A. TEUKOLSKY, W. T. VETTERLING, AND B. P. FLANNERY. 1992. *Numerical recipes in FORTRAN*. Cambridge Univ. Press.
- SMEATHERS, J. E., AND J. F. V. VINCENT. 1979. Mechanical properties of mussel byssus threads. *J. Moll. Stud.* **45**: 219–230.
- SOUSA, W. P. 1979a. Disturbance in marine intertidal boulder fields: The nonequilibrium maintenance of species diversity. *Ecology* **60**: 1225–1239.
- . 1979b. Experimental investigations of disturbance and ecological succession in a rocky intertidal algal community. *Ecol. Monogr.* **49**: 227–254.
- THOMSON, W. T. 1993. *Theory of vibrations with applications*. 4th Ed. Prentice-Hall.
- UTTER, B. D., AND M. W. DENNY. 1996. Wave induced forces on the giant kelp *Macrocystis pyrifera* (Agardh): Field test of a computational model. *J. Exp. Biol.* **199**: 2645–2654.
- VINCENT, J. F. V. 1982. *Structural biomaterials*. Rev. Ed. Princeton Univ. Press.
- VOGEL, S. 1994. *Life in moving fluids*. 2nd Ed. Princeton Univ. Press.
- YOUNG, G. A. 1985. Byssus-thread formation by the mussel *Mytilus edulis*: Effects of environmental factors. *Mar. Ecol. Prog. Ser.* **24**: 261–271.

Received: 2 May 1997

Accepted: 10 December 1997